LETTER

https://doi.org/10.1038/s41586-018-0274-0

Majorana quantization and half-integer thermal quantum Hall effect in a Kitaev spin liquid

Y. Kasahara[1], T. Ohnishi[1], Y. Mizukami[2], O. Tanaka[2], Sixiao Ma[1], K. Sugii[3], N. Kurita[4], H. Tanaka[4], J. Nasu[4], Y. Motome[5], T. Shibauchi[2] & Y. Matsuda[1]*

The quantum Hall effect in two-dimensional electron gases involves the flow of topologically protected dissipationless charge currents along the edges of a sample. Integer or fractional electrical conductance is associated with edge currents of electrons or quasiparticles with fractional charges, respectively. It has been predicted that quantum Hall phenomena can also be created by edge currents with a fundamentally different origin: the fractionalization of quantum spins. However, such quantization has not yet been observed. Here we report the observation of this type of quantization of the Hall effect in an insulating two-dimensional quantum magnet[1], α-$RuCl_3$, with a dominant Kitaev interaction (a bond-dependent Ising-type interaction) on a two-dimensional honeycomb lattice[2–7]. We find that the application of a magnetic field parallel to the sample destroys long-range magnetic order, leading to a field-induced quantum-spin-liquid ground state with substantial entanglement of local spins[8–12]. In the low-temperature regime of this state, the two-dimensional thermal Hall conductance reaches a quantum plateau as a function of the applied magnetic field and has a quantization value that is exactly half of the two-dimensional thermal Hall conductance of the integer quantum Hall effect. This half-integer quantization of the thermal Hall conductance in a bulk material is a signature of topologically protected chiral edge currents of charge-neutral Majorana fermions (particles that are their own antiparticles), which have half the degrees of freedom of conventional fermions[13–16]. These results demonstrate the fractionalization of spins into itinerant Majorana fermions and Z_2 fluxes, which is predicted to occur in Kitaev quantum spin liquids[1,3]. Above a critical magnetic field, the quantization disappears and the thermal Hall conductance goes to zero rapidly, indicating a topological quantum phase transition between the states with and without chiral Majorana edge modes. Emergent Majorana fermions in a quantum magnet are expected to have a great impact on strongly correlated quantum matter, opening up the possibility of topological quantum computing at relatively high temperatures.

Topological states of matter are described in terms of topological invariant quantities whose values are quantized. The quantity most frequently used to prove the existence of these states is the electrical Hall conductivity. In the quantum Hall state, the Hall conductance σ_{xy}^{2D} is quantized in units of $e^2/2\pi\hbar$, where e is the electronic charge and $\hbar$ is the Planck constant, as $\sigma_{xy}^{2D} = q\,(e^2/2\pi\hbar)$; q is an integer in the integer quantum Hall effect (QHE) and a fraction in the fractional QHE where, with very few exceptions, it has an odd denominator. These quantizations attest to topologically ordered states. Another topological invariant in the topological phase is the two-dimensional (2D) thermal Hall conductance. The thermal Hall conductivity per 2D sheet, κ_{xy}^{2D}, is quantized in units of $(\pi/6)\,(k_B^2/\hbar)\,/T$, where k_B is the Boltzmann constant and T is the temperature, as

$$\kappa_{xy}^{2D}/T = q(\pi/6)(k_B^2/\hbar) \quad (1)$$

Although the thermal Hall conductivity is much harder to measure than electrical Hall conductivity, it has a clear advantage in revealing the topological phases possessing charge-neutral excitations that cannot be detected by the electrical Hall conductivity. In particular, a $q = 1/2$ state with positive thermal Hall sign is a decisive manifestation of the charge-neutral edge currents of Majorana particles (Fig. 1a, b), distinguishing unambiguously between different candidate topological orders. We note that a Majorana quantized phase characterized by $q = 1/2$ has been predicted in chiral topological superconductors[13–15]. However, as the topological superconductivity in bulk materials has not been fully established, previous experiments searching for Majorana fermions have focused on the proximity effect between conventional superconductors and nanowires or topological materials[17–20]. Here we present a fundamentally different approach to this issue and perform direct measurements of the thermal Hall conductance in a bulk insulating magnet.

Systems composed of interacting 1/2 spins on a honeycomb lattice with bond-directional exchange interactions J_K are of great interest because they host quantum-spin-liquid (QSL) ground states where topological excitations emerge[1]. Such Kitaev QSLs exhibit two types of fractionalized quasiparticle excitation, that is, itinerant (mobile) Majorana fermions and Z_2 fluxes with a gap. The Majorana fermion has a massless (gapless) Dirac-type dispersion in zero field. In magnetic fields, a Majorana fermion system characterized by the bulk gap and gapless edge modes has been realized[1,3], and the Z_2 flux obeys anyonic statistics.

Recently, a strongly spin–orbit-coupled Mott insulator, α-$RuCl_3$, has emerged as a prime candidate for hosting an approximate Kitaev QSL. In this compound, local $j_{eff} = 1/2$ pseudospins are almost coplanar within the 2D honeycomb layer and the Kitaev interaction, $J_K/k_B \approx 80$ K, has an important role[5–7]. The system is in a spin-liquid (Kitaev paramagnetic) state below about J_K/k_B and shows antiferromagnetic (AFM) order with zigzag spin structure[21] (Fig. 1c) at the Néel temperature $T_N \approx 7$ K due to non-Kitaev interactions, such as Heisenberg exchange and off-diagonal interactions. The thermal Hall conductance of α-$RuCl_3$ has been measured in a magnetic field perpendicular to the 2D planes[22]. For this geometry, a finite positive κ_{xy}/T emerges in the spin-liquid regime, at $T_N < T \lesssim 80$ K. On entering the AFM state, κ_{xy}/T changes sign and its magnitude is strongly suppressed. The quantization and plateau behaviour of κ_{xy}^{2D}/T have not been observed in the spin-liquid regime. Therefore, expanding the measurements to a lower-temperature region in the liquid state is crucial.

The response of α-$RuCl_3$ to magnetic fields is highly anisotropic, with largely different in-plane and out-of plane properties[8,11,12,23,24]. It has been reported that although T_N is minimally influenced by an external magnetic field perpendicular to the 2D plane, it is markedly suppressed by a parallel field. This highly anisotropic response is confirmed by measurements of the longitudinal thermal conductivity, κ_{xx}, with the heat current along the a axis in a magnetic field $\boldsymbol{H}$ applied along various directions in the a–c plane, as shown in the inset of

[1]Department of Physics, Kyoto University, Kyoto, Japan. [2]Department of Advanced Materials Science, University of Tokyo, Chiba, Japan. [3]Institute for Solid State Physics, University of Tokyo, Chiba, Japan. [4]Department of Physics, Tokyo Institute of Technology, Tokyo, Japan. [5]Department of Applied Physics, University of Tokyo, Tokyo, Japan. *e-mail: matsuda@scphys.kyoto-u.ac.jp

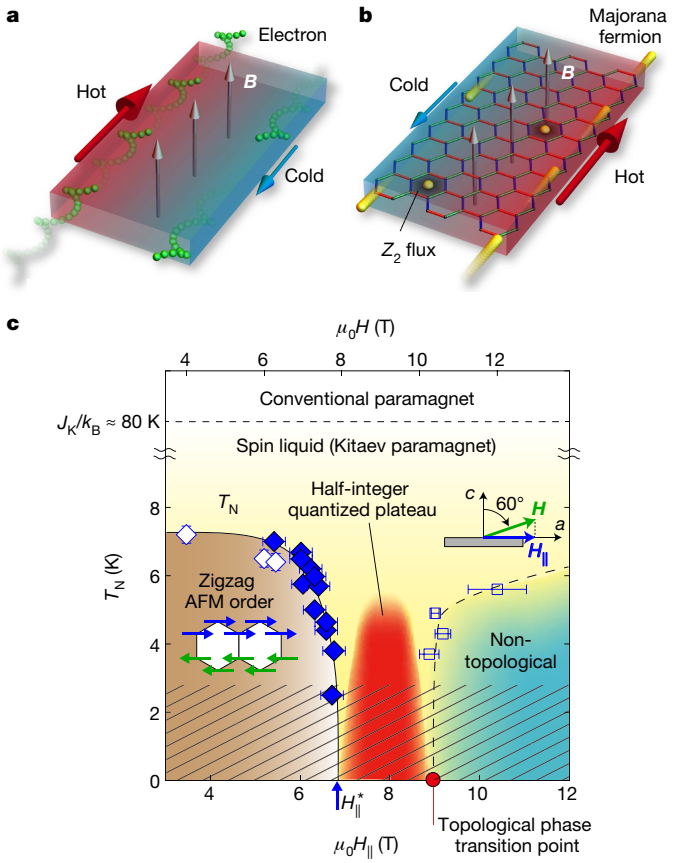

Fig. 1 | Chiral Majorana edge currents and temperature–magnetic field phase diagram of α-$RuCl_3$. **a**, **b**, Schematic illustrations of heat conduction in the integer quantum Hall state of a 2D electron gas (**a**) and a Kitaev QSL state (**b**) in a magnetic field perpendicular to the sample plane (grey arrows). In the red (blue) area, the temperature is higher (lower), and the red and blue arrows represent thermal flow. In the quantum Hall state, the skipping orbits of electrons (green spheres) at the edge, which form one-dimensional edge channels, conduct heat and κ_{xy} is negative in sign. In the Kitaev QSL state, spins are fractionalized into Majorana fermions (yellow spheres) and Z_2 fluxes (hexagons). The heat is carried by chiral edge currents of charge-neutral Majorana fermions and κ_{xy} is positive in sign. **c**, Phase diagram of α-$RuCl_3$ in a field tilted at $\theta = 60°$ (see right inset, where green and blue arrows represent the magnetic field $\boldsymbol{H}$ and parallel field component $H_\parallel$). Open and closed diamonds represent the onset temperature of AFM order with zigzag-type T_N determined by the T and H dependences of κ_{xx}, respectively (see Fig. 2b and Extended Data Figs. 1 and 2). Below $T \approx J_K/k_B \approx 80$ K, the spin-liquid (Kitaev paramagnetic) state appears. At $\mu_0 H_\parallel^* \approx 7$ T, T_N vanishes. A half-integer quantized plateau of the 2D thermal Hall conductance is observed in the red area. Open blue squares represent the fields where the thermal Hall response disappears. The red circle is the suggested topological phase-transition point that separates the non-trivial QSL state with topologically protected chiral Majorana edge currents from a trivial state, such as a non-topological spin liquid. The striped region denotes the region that was not accessible in the thermal Hall effect measurements. Error bars represent one standard deviation (error bars for the temperature are smaller than the symbols). The left inset shows the zigzag magnetic structure in the AFM state. The magnetic moments of Ru atoms represented by blue and green arrows are aligned antiparallel.

Fig. 2a, where $H_\parallel = H\sin\theta$ and $H_\perp = H\cos\theta$ are the field components parallel and perpendicular to the a axis, respectively, and θ is the angle between $\boldsymbol{H}$ and the c axis. In zero field, κ_{xx} exhibits a distinct kink at T_N, as shown in Fig. 2a. Although this kink is observed in a perpendicular field ($\theta = 0°$) of 12 T at the same temperature, no such anomaly is observed in a parallel field[11,12] ($\theta = 90°$) of 7 T. In Fig. 2a, we also plot κ_{xx} in an applied magnetic field of 8 T, tilted away from the c axis ($\theta = 60°$, $\mu_0 H_\parallel \approx 7$ T). As in the case of the parallel field, no kink is observed. Figure 1c displays the phase diagram of an α-$RuCl_3$ sample in a tilted field of $\theta = 60°$, where T_N is plotted as a function of $H_\parallel$. The inset of Fig. 2b shows T_N plotted as a function of $H_\parallel$ for $\theta = 45°$, 60° and 90°. For $\theta = 60°$, T_N agrees well with that for 90° and vanishes at the same critical field of $\mu_0 H_\parallel^* \approx 7$ T, whereas for 45° T_N vanishes at $\mu_0 H_\parallel \approx 6$ T. Although T_N does not scale perfectly with $H_\parallel$, these results demonstrate the quasi-2D nature of the magnetic properties. In stark contrast to the strong out-of-plane (a–c) anisotropy, the in-plane (a–b) anisotropy is very small (Extended Data Fig. 3a–c).

Above $H_\parallel = H_\parallel^*$, where the AFM order melts, the presence of a peculiar spin-liquid state has been suggested on the basis of nuclear magnetic resonance and neutron scattering measurements; the former show the presence of a spin gap[25] and the latter reveal unusual continuous spin excitations[26]. These magnetic properties are consistent with those expected in a Kitaev-type spin-liquid state.

To study the thermal Hall effect in the spin-liquid state above $H_\parallel = H_\parallel^*$, κ_{xy} is measured by sweeping fields in tilted directions and obtained by anti-symmetrizing the thermal response of the sample with respect to the field direction. In this configuration, the Hall response is determined by $H_\perp$. Because the magnitude of κ_{xy} is extremely small compared to κ_{xx} in α-$RuCl_3$, special care is taken to detect the intrinsic thermal Hall signal (see Methods). Figure 3a–d and Fig. 3e–h depict κ_{xy}/T at $\theta = 60°$ and 45°, respectively, plotted as a function of $H_\perp$ above $H_\parallel = H_\parallel^*$ at low temperatures. The experimental error in the detection of the temperature difference between Hall contacts becomes considerable below 3.5 K, leading to unreliable determination of κ_{xy} in our setup.

In the AFM state, κ_{xy}/T is extremely small (see Extended Data Fig. 4). Upon entering the field-induced spin-liquid state, κ_{xy}/T, which is positive in sign, increases rapidly. The most striking feature is that κ_{xy}/T exhibits a plateau in the field range of 4.5 T $< \mu_0 H_\perp <$ 4.8–5.0 T for $\theta = 60°$ and 6.8 T $< \mu_0 H_\perp <$ 7.2–7.4 T for $\theta = 45°$, as shown in Fig. 3a–c and Fig. 3e–g, respectively. The right axes represent κ_{xy}^{2D}/T in units of quantum thermal Hall conductance $(\pi/6)(k_B^2/\hbar)$, where $\kappa_{xy}^{2D} = \kappa_{xy} d$ with a layer distance[21] of $d = 5.72$ Å. Remarkably, the plateau is very close to the half of the quantum thermal Hall conductance reported in the integer quantum Hall system[27] within the error of 3%, demonstrating the emergence of a half-integer thermal Hall conductance plateau. Above $\mu_0 H_\perp \approx 5.0$ T for $\theta = 60°$ (7.4 T for $\theta = 45°$), κ_{xy}^{2D}/T decreases rapidly and vanishes. We note that the half-integer quantized plateau is reproduced in crystal from different growth (Extended Data Fig. 5). Although the plateau behaviour seems to be preserved at 5.6 K, κ_{xy}^{2D}/T slightly deviates from the quantized value. At higher temperatures, the plateau behaviour disappears (Fig. 3d, h).

The temperature dependence of κ_{xy}/T at magnetic fields where a plateau is observed is shown in Fig. 4. The half-integer thermal Hall conductance is observable up to about 5.5 K, above which κ_{xy}/T increases rapidly with T. As shown in the inset of Fig. 4, κ_{xy}/T decreases after reaching a maximum at around 15 K and nearly vanishes above about 60 K (see Extended Data Fig. 6). As the vanishing temperature of κ_{xy}/T is close to the Kitaev interaction, it is natural to consider that the finite thermal Hall signal reflects unusual quasiparticle excitations inherent to the spin-liquid state governed by the Kitaev interaction (see Methods for further discussion).

In equation (1), the coefficient q gives the chiral central charge of the gapless boundary modes, which propagate along one direction. The central charge represents a degree of freedom of one-dimensional gapless modes; it is unity for conventional fermions and 1/2 for Majorana fermions whose degrees of freedom are half of those of conventional fermions. An integer quantum Hall system with bulk Chern number ν has ν boundary modes with $q = \nu$, whereas a Kitaev QSL with Chern number ν has ν Majorana boundary modes with $q = \nu/2$. Thus, the observed half-integer thermal Hall conductance provides direct evidence of chiral Majorana edge currents. We also note that the positive Hall sign is also consistent with that predicted in the Kitaev QSL[1]. In the pure Kitaev model, the excitation energy of the Z_2 flux is estimated[7] to be $\Delta_F/k_B \approx 0.06 J_K/k_B \approx 5.5$ K. Recent numerical results[16] of the thermal

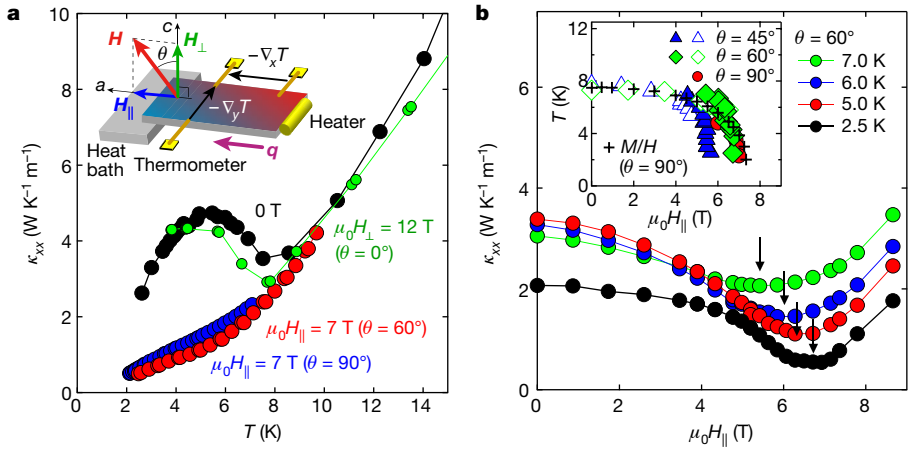

Fig. 2 | Longitudinal thermal conductivity in α-RuCl$_3$. a, Temperature dependence of κ_{xx} in a magnetic field $\boldsymbol{H}$ applied along various directions in the a–c plane. The inset illustrates a schematic of the measurement setup for κ_{xx} and κ_{xy} (see Methods for details). **b**, κ_{xx} at $\theta = 60°$, plotted as a function of the parallel field component, $H_{\parallel}$. The inset shows T_N versus $H_{\parallel}$ at different field directions. T_N is determined by the T dependence of κ_{xx} shown in **a** (open symbols) and by the minimum in the H dependence of κ_{xx} (filled symbols), shown by arrows in the main panel. Crosses show T_N for $\theta = 90°$, determined from magnetic susceptibility (M/H, where M is the magnetization) measurements[26].

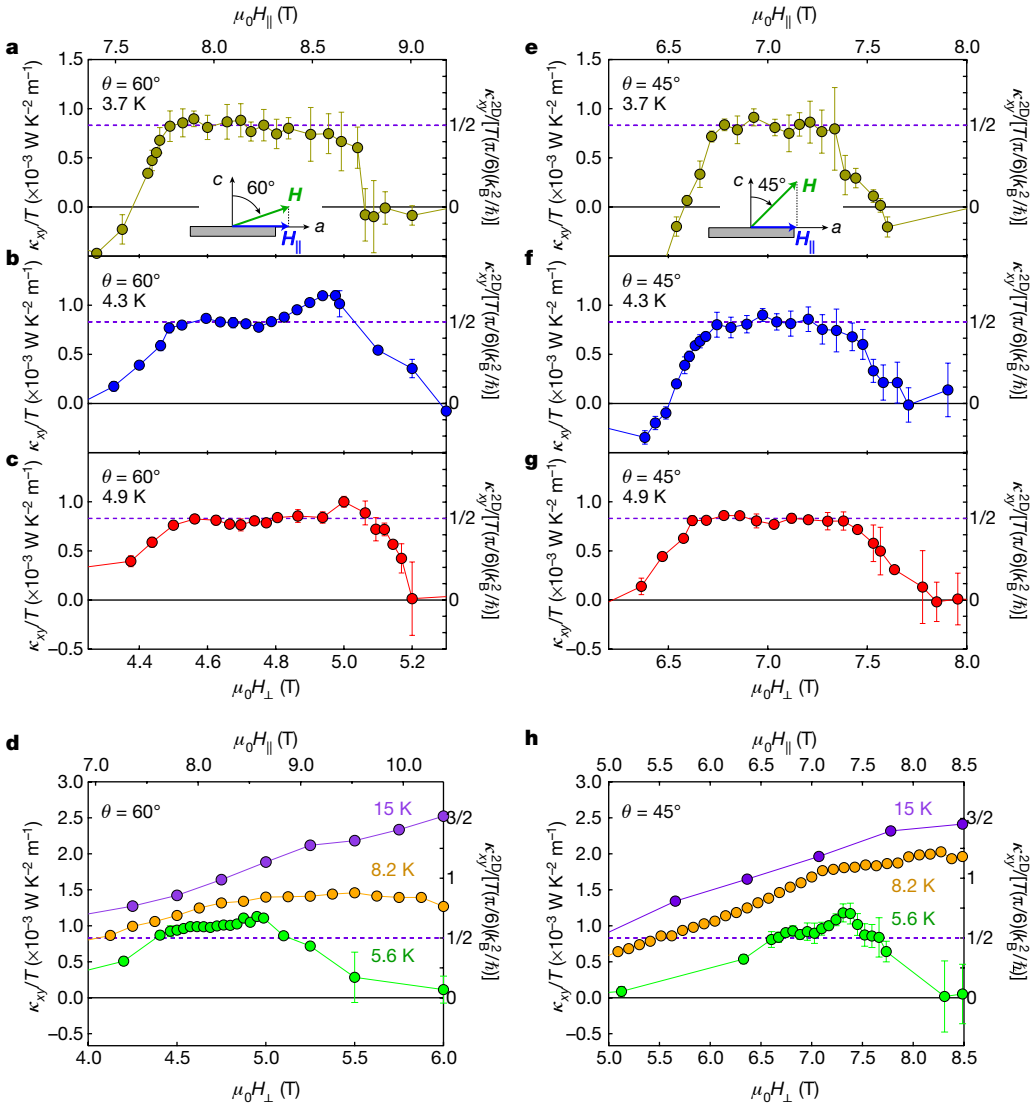

Fig. 3 | Half-integer thermal Hall conductance plateau. a–**h**, Thermal Hall conductivity κ_{xy}/T in a field tilted at $\theta = 60°$ (**a**–**d**) and 45° (**e**–**h**) plotted as a function of $H_{\perp}$ (see inset of Fig. 2a). The top axes show the parallel field component, $H_{\parallel}$. The right scales represent the 2D thermal Hall conductance, κ_{xy}^{2D}/T, in units of $(\pi/6)(k_B^2/\hbar)$. Violet dashed lines represent the half-integer thermal Hall conductance, $\kappa_{xy}^{2D}/[T(\pi/6)(k_B^2/\hbar)] = 1/2$. Error bars represent one standard deviation.

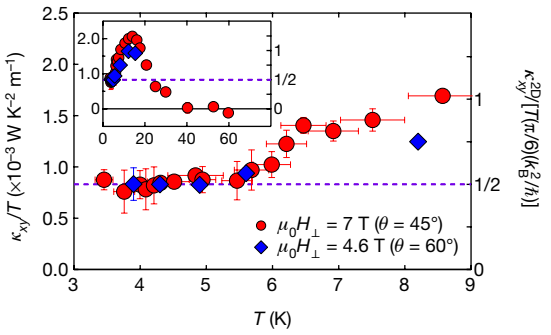

Fig. 4 | Temperature dependence of the thermal Hall conductance. The main panel shows κ_{xy}/T in fields tilted at $\theta = 45°$ and 60° (see inset of Fig. 2a) at $\mu_0 H_\perp = 7$ T and 4.6 T, respectively, where a quantized thermal Hall conductance plateau is observed at low temperatures. The right scale is the 2D thermal Hall conductance κ_{xy}^{2D}/T in units of $(\pi/6)(k_B^2/\hbar)$. The violet dashed line represents the half-integer thermal Hall conductance, $\kappa_{xy}^{2D}/[T(\pi/6)(k_B^2/\hbar)] = 1/2$. The inset shows the same data in a wider temperature regime. Error bars represent one standard deviation.

Hall conductance for the 2D pure Kitaev model calculated with the quantum Monte Carlo method show that quantization occurs slightly below Δ_F/k_B. Experimentally, Δ_F/k_B is estimated[25] to be 10 K, which is consistent with the persistence of the thermal Hall quantization up to around 5 K.

In the plateau regime of κ_{xy}, no anomaly is observed in κ_{xx}, probably because phonon contributions largely dominate over fermionic excitations arising from spins in κ_{xx} in the whole temperature range[28,29]. Moreover, owing to the strong spin–phonon coupling in α-$RuCl_3$[11], the phonon conductivity is expected to show complicated H and T dependences. The observed behaviour of the plateau as a function of H and T therefore demonstrates that κ_{xy}/T is not affected by spin–phonon scattering in the plateau regime, providing strong support for topological protection. The fact that κ_{xy} vanishes at the highest fields, as shown in Fig. 3a–c, e–g, provides direct evidence that the thermal Hall effect is not influenced by phonons, demonstrating that κ_{xy} is a unique and powerful probe in the search for Majorana quantization.

We stress that a half-integer thermal Hall conductance in a bulk material is a direct consequence of the chiral Majorana edge current. Recent experiments based on the proximity effect between a quantum anomalous Hall insulator and a conventional superconductor have reported a signature of chiral Majorana edge modes[20]. However, this is based on the observation of half-integer quantization of the longitudinal electrical conductance via the scattering matrix effect between the edge states of the insulator and superconductor. Moreover, Majorana fermions in Kitaev magnets and topological superconductors have essentially different features. In the former, strong correlations give rise to Majorana fermions, whereas in the latter they do not play a role. In addition, Majorana fermions exist inside the bulk of a sample in the Kitaev QSL state, in sharp contrast to topological superconductors, where they appear only at the edges. This distinct nature of Majorana fermions is supported by the fact that the quantum plateau disappears below about 400 mK in a topological superconductor device[20], whereas it is preserved up to around 5 K in α-$RuCl_3$.

At $\theta = 60°$, $\kappa_{xy}^{2D}(H)/T$ increases slightly from the quantized value before going to zero at a high field at 4.3 K and 4.9 K, which is reproduced in a different crystal (Extended Data Fig. 5a). However, such a behaviour is not observed at $\theta = 45°$. On the other hand, an overshoot is also observed in the temperature dependence of κ_{xy}^{2D}, irrespective of the angle (Fig. 4) and crystal (Extended Data Fig. 5b); therefore, there seem to be certain high-energy corrections that are responsible for the excess conductivity at high fields and high temperatures. These overshoots are in contrast to the numerical results of the thermal Hall effect for the 2D pure Kitaev model with a weak magnetic field[16]. Meanwhile, it has been pointed out that non-Kitaev interactions, such as Heisenberg and off-diagonal ones, are important for α-$RuCl_3$[30,31]. Hence, the discrepancy may be attributed to high-field effects or non-Kitaev interactions, which deserves further study.

The near vanishing of κ_{xy}^{2D}/T after its rapid suppression in the high-field regime (Fig. 3a–c, e–g) demonstrates the disappearance of chiral Majorana edge currents. As shown by the open blue square in Fig. 1c, the temperature at which κ_{xy}^{2D}/T vanishes decreases rapidly with decreasing $H_\parallel$. This suggests a topological quantum phase transition from the non-trivial QSL to a trivial high-field state, where the thermal Hall effect is absent, at $\mu_0 H_\parallel \approx 9$ T, as shown by the red circle in Fig. 1c[32]. The specific heat at 0.47 K for $\theta = 60°$ exhibits a dip-like anomaly in the vicinity of 9 T, which can be associated with an abrupt change of the spin gap at the topological transition, strongly supporting the presence of a characteristic field revealed by κ_{xy}/T (Extended Data Fig. 7a–c). The vanishing of κ_{xy}/T at the highest fields is unlikely to be due to the crossover to a simple forced ferromagnetic state because the magnetization at 9 T is less than 1/3 of the fully polarized value, indicating that paramagnetic spins still remain. The observation of half-integer thermal Hall conductance reveals that topologically protected chiral Majorana edge currents persist in α-$RuCl_3$, even in the presence of non-Kitaev interactions and a parallel field. This observation opens a possibility of using Majorana fermions and their link to non-Abelian anyons, which are important for topological quantum computing, revealing novel aspects of strongly correlated topological quantum matters.

Online content

Any Methods, including any statements of data availability and Nature Research reporting summaries, along with any additional references and Source Data files, are available in the online version of the paper at https://doi.org/10.1038/s41586-018-0274-0.

Received: 13 November 2017; Accepted: 24 April 2018;
Published online 11 July 2018.

1. Kitaev, A. Anyons in an exactly solved model and beyond. *Ann. Phys.* **321**, 2–111 (2006).
2. Jackeli, G. & Khaliullin, G. Mott insulators in the strong spin–orbit coupling limit: from Heisenberg to a quantum compass and Kitaev models. *Phys. Rev. Lett.* **102**, 017205 (2009).
3. Trebst, S. Kitaev materials. Preprint at https://arxiv.org/abs/1701.07056 (2017).
4. Kim, H.-S., Shankar, V. V., Catuneanu, A. & Kee, H.-Y. Kitaev magnetism in honeycomb $RuCl_3$ with intermediate spin–orbit coupling. *Phys. Rev. B* **91**, 241110 (2015).
5. Banerjee, A. et al. Proximate Kitaev quantum spin liquid behaviour in a honeycomb magnet. *Nat. Mater.* **15**, 733–740 (2016).
6. Sandilands, L. J., Tian, Y., Plumb, W., Kim, Y.-J. & Burch, K. S. scattering continuum and possible fractionalized excitations in α-$RuCl_3$. *Phys. Rev. Lett.* **114**, 147201 (2015).
7. Nasu, J., Knolle, J., Kovrizhin, D. L., Motome, Y. & Moessner, R. Fermionic response from fractionalization in an insulating two-dimensional magnet. *Nat. Phys.* **12**, 912–915 (2016).
8. Yadav, R. et al. Kitaev exchange and field-induced quantum spin-liquid states in honeycomb α-$RuCl_3$. *Sci. Rep.* **6**, 37925 (2016).
9. Baek, S.-H. et al. Evidence for a field-induced quantum spin liquid in α-$RuCl_3$. *Phys. Rev. Lett.* **119**, 037201 (2017).
10. Wolter, A. U. B. et al. Field-induced quantum criticality in the Kitaev system α-$RuCl_3$. *Phys. Rev. B* **96**, 041405 (2017).
11. Leahy, I. A. et al. Anomalous thermal conductivity and magnetic torque response in the honeycomb magnet α-$RuCl_3$. *Phys. Rev. Lett.* **118**, 187203 (2017).
12. Hentrich, R. et al. Unusual phonon heat transport in α-$RuCl_3$: strong spin–phonon scattering and field-induced spin gap. *Phys. Rev. Lett.* **120**, 117204 (2018).
13. Read, N. & Green, D. Paired states of fermions in two dimensions with breaking of parity and time-reversal symmetries and the fractional quantum Hall effect. *Phys. Rev. B* **61**, 10267–10297 (2000).
14. Sumiyoshi, H. & Fujimoto, S. Quantum thermal hall effect in a time-reversal-symmetry- broken topological superconductor in two dimensions: approach from bulk calculations. *J. Phys. Soc. Jpn.* **82**, 023602 (2013).
15. Nomura, K., Ryu, S., Furusaki, A. & Nagaosa, N. Cross-correlated responses of topological superconductors and superfluids. *Phys. Rev. Lett.* **108**, 026802 (2012).
16. Nasu, J., Yoshitake, J. & Motome, Y. Thermal transport in the Kitaev model. *Phys. Rev. Lett.* **119**, 127204 (2017).
17. Mourik, V. et al. Signatures of Majorana fermions in hybrid superconductor-semiconductor nanowire devices. *Science* **336**, 1003–1007 (2012).

18. Nadj-Perge, S. et al. Observation of Majorana fermions in ferromagnetic atomic chains on a superconductor. *Science* **346**, 602–607 (2014).
19. Das, A. et al. Zero-bias peaks and splitting in an Al-InAs nanowire topological superconductor as a signature of Majorana fermions. *Nat. Phys.* **8**, 887–895 (2012).
20. He, Q. L. et al. Chiral Majorana fermion modes in a quantum anomalous Hall insulator- superconductor structure. *Science* **357**, 294–299 (2017).
21. Johnson, R. D. et al. Monoclinic crystal structure of α-$RuCl_3$ and the zigzag antiferromagnetic ground state. *Phys. Rev. B* **92**, 235119 (2015).
22. Kasahara, Y. et al. Unusual thermal Hall effect in a Kitaev spin liquid candidate α-$RuCl_3$. *Phys. Rev. Lett.* **120**, 217205 (2018).
23. Majumder, M., Schmidt, M., Rosner, H., Tsirlin, A. A., Yasuoka, H. & Baenitz, M. Anisotropic Ru^{3+} $4d^5$ magnetism in the α-$RuCl_3$ honeycomb system: susceptibility, specific heat, and zero-field NMR. *Phys. Rev. B* **91**, 180401 (2015).
24. Chaloupka, L. & Khaliullin, G. Magnetic anisotropy in the Kitaev model systems Na2IrO3 and RuCl3. *Phys. Rev. B* **94**, 064435 (2016).
25. Janša N. et al. Observation of two types of fractional excitation in the Kitaev honeycomb magnet. *Nat. Phys*. https://doi.org/10.1038/s41567-018-0129-5 (2018).
26. Banerjee, A. et al. Excitations in the field-induced quantum spin liquid state of α-RuCl3. *npj Quantum Mater.* **3**, 8 (2018).
27. Banerjee, M. et al. Observed quantization of anyonic heat flow. *Nature* **545**, 75–79 (2017).
28. Hirobe, D., Sato, M., Shiomi, Y., Tanaka, H. & Saitoh, E. Magnetic thermal conductivity far above the Néel temperatures in the Kitaev-magnet candidate α-$RuCl_3$. *Phys. Rev. B* **95**, 241112 (2017).
29. Yu, Y. J. et al. Ultralow-temperature thermal conductivity of the Kitaev honeycomb magnet α-$RuCl_3$ across the field-induced phase transition. *Phys. Rev. Lett.* **120**, 067202 (2018).
30. Gohlke, M., Wachtel, G., Yamaji, Y., Pollmann, F. & Kim, Y. B. Signatures of quantum spin liquid in Kitaev-like frustrated magnets. *Phys. Rev. B* **97**, 075126 (2018).
31. Winter, S. M., Li, Y., Jeschke, H. O. & Valenti, R. Challenges in design of Kitaev materials: magnetic interactions from competing energy scales. *Phys. Rev. B* **93**, 214431 (2016).
32. Jiang, H.-C., Gu, Z.-C., Qi, X.-L. & Trebst, S. Possible proximity of the Mott insulating iridate Na_2IrO_3 to a topological phase: Phase diagram of the Heisenberg-Kitaev model in a magnetic field. *Phys. Rev. B* **83**, 245104 (2011).

Acknowledgements We thank S. Fujimoto, H. Ishizuka, N. Kawakami, H.-Y. Kee, Y. B. Kim, E.-G. Moon, N. P. Ong, M. Shimozawa, M. Udagawa and M. Yamashita for useful discussions. We thank N. Abe, Y. Tokunaga and T. Arima for support in X-ray diffraction measurements. This work was supported by Grants-in-Aid for Scientific Research (KAKENHI) (numbers 25220710, 15H02014, 15H02106, 15H05457, 15K13533, 15K17692, 16H02206, 16H00987, 16K05414, 17H01142 and 18H04223) and Grants-in-Aid for Scientific Research on innovative areas "Topological Materials Science" (number JP15H05852) from Japan Society for the Promotion of Science (JSPS).

Reviewer information *Nature* thanks K.-Y. Choi, K. Shtengel and the other anonymous reviewer(s) for their contribution to the peer review of this work.

Author contributions Y.K. and Y. Matsuda conceived and designed the study. Y.K., T.O. and S.M. performed the thermal transport measurements. Y. Mizukami, O.T. and K.S. performed the specific heat measurements. N.K. and H.T. synthesized the high-quality single crystalline samples. Y.K., T.O., J.N., Y. Motome, T.S. and Y. Matsuda discussed the results. Y.K., J.N., Y. Motome, T.S. and Y. Matsuda prepared the manuscript.

Competing interests The authors declare no competing interests.

Additional information
Extended data is available for this paper at https://doi.org/10.1038/s41586-018-0274-0.
Reprints and permissions information is available at http://www.nature.com/reprints.
Correspondence and requests for materials should be addressed to Y.M.
Publisher's note: Springer Nature remains neutral with regard to jurisdictional claims in published maps and institutional affiliations.

METHODS

Single-crystal growth. High-quality single crystals of α-$RuCl_3$ were grown by a vertical Bridgman method as described in ref. [33]. For thermal transport measurements, we carefully picked up thin crystals with a plate-like shape. Typical sample size was roughly 2 mm × 0.5 mm × 0.02 mm. We selected the best crystals, in which no anomaly associated with the magnetic transition at 14 K due to the stacking faults was detected by magnetic susceptibility, specific heat and thermal transport measurements.

Thermal transport measurements. Thermal and thermal Hall conductivities were measured simultaneously on the same crystal by the standard steady-state method, using the experimental setup illustrated in the inset of Fig. 2a. A heat current $\boldsymbol{q}$ was applied along the a axis ($\boldsymbol{q} \parallel \boldsymbol{x}$). Using special jigs, a magnetic field $\boldsymbol{H}$ was applied along various directions in the a–c plane within an accuracy of less than one degree. The temperature gradient $-\nabla_x T \parallel \boldsymbol{x}$ and $-\nabla_y T \parallel \boldsymbol{y}$ was measured by carefully calibrated Cernox thermometers. The sample temperature was measured with an accuracy of 0.1 mK using alternating current resistance bridges. A 1-kΩ chip resistor was used to generate the heat current. The magnitude of the thermal gradient was less than 5% of the base temperature. To reduce the noise level, all measurements were performed in a radio-frequency-shielded room. For the measurements of the thermal Hall effect, we removed the longitudinal response due to misalignment of the contacts by anti-symmetrizing the measured $\nabla_y T$ as $\nabla_y T^{\mathrm{asym}}(H) = [\nabla_y T(H) - \nabla_y T(-H)]/2$ at each temperature. We note that the offset transverse thermal gradient due to the misalignment of the Hall contact was reduced to be less than 0.5% of the longitudinal thermal gradient in zero field. κ_{xx} and κ_{xy} were obtained from the longitudinal thermal resistivity, $w_{xx} = \nabla_x T/q$, and the thermal Hall resistivity, $w_{xy} = \nabla_y T^{\mathrm{asym}}/q$, as $\kappa_{xx} = w_{xx}/(w_{xx}^2 + w_{xy}^2)$ and $\kappa_{xx} = w_{xy}/(w_{xx}^2 + w_{xy}^2)$. To avoid a background Hall signal, a LiF heat bath and non-metallic grease were used. We confirmed that the thermal Hall signal in LiF is negligibly small within our experimental resolution[34]. The experimental error in determining κ_{xy}, caused by the uncertainty in measuring the distance between the contacts and the thickness of the crystal, is within ±2%.

Specific heat measurements. Specific heat was measured by a long relaxation method[35] in a ^{3}He cryostat. A Cernox chip resistor was used as both a thermometer and a heater. The sample was attached to the calorimeter using grease. The thermometer was calibrated in magnetic field of up to 12 T.

Origin of thermal Hall response. Here we discuss κ_{xy}/T in the high-temperature spin-liquid regime, where no plateau behaviour is observed. A finite κ_{xy}/T in the spin-liquid states has been reported only in the kagomé insulator volborthite $Cu_3V_2O_7(OH)_2{\cdot}2H_2O$ so far[34]. We point out that the behaviour of κ_{xy}/T in the high-temperature regime of α-$RuCl_3$ is essentially different from that in the liquid state of volborthite; the κ_{xy} value of volborthite is opposite in sign to that of α-$RuCl_3$ and its magnitude is more than one order magnitude smaller. Until now, all theories except the Kitaev model predict that a finite κ_{xy} can appear in spin-liquid states when the Dzyaloshinsky–Moriya (DM) interaction is present[36]. In fact, volborthite has a large DM interaction. However, the DM interaction in α-$RuCl_3$ is approximately 5 K, which is much smaller[31] than J_K, and hence it does not play an important role at high temperatures. Moreover, the phonon thermal Hall conductivity is three orders of magnitude smaller than the observed κ_{xy}/T in the spin-liquid state and shows essentially different temperature dependence[37].

Data availability. The data that support the results presented in this paper and other findings of this study are available from the corresponding author upon reasonable request.

33. Kubota, Y., Tanaka, H., Ono, T., Narumi, Y. & Kindo, K. Successive magnetic phase transition in α-$RuCl_3$: XY-like frustrated magnet on the honeycomb lattice. *Phys. Rev. B* **91**, 094422 (2015).
34. Watanabe, D. et al. Emergence of nontrivial magnetic excitations in a spin liquid state of kagomé volborthite. *Proc. Natl Acad. Sci. USA* **113**, 8653–8657 (2016).
35. Taylor, O. J., Carrington, A. & Schlueter, J. A. Specific-heat measurements of the gap structure of the organic superconductor κ-$(ET)_2Cu[N(CN)_2]Br$ and κ-$(ET)_2Cu(NCS)_2$. *Phys. Rev. Lett.* **99**, 057001 (2007).
36. Han, J. H. & Lee, H. Spin chirality and Hall-like transport phenomena of spin excitations. *J. Phys. Soc. Jpn* **86**, 011007 (2017).
37. Sugii, K. et al. Thermal Hall effect in a phonon-glass $Ba_3CuSb_2O_9$. *Phys. Rev. Lett.* **118**, 145902 (2017).

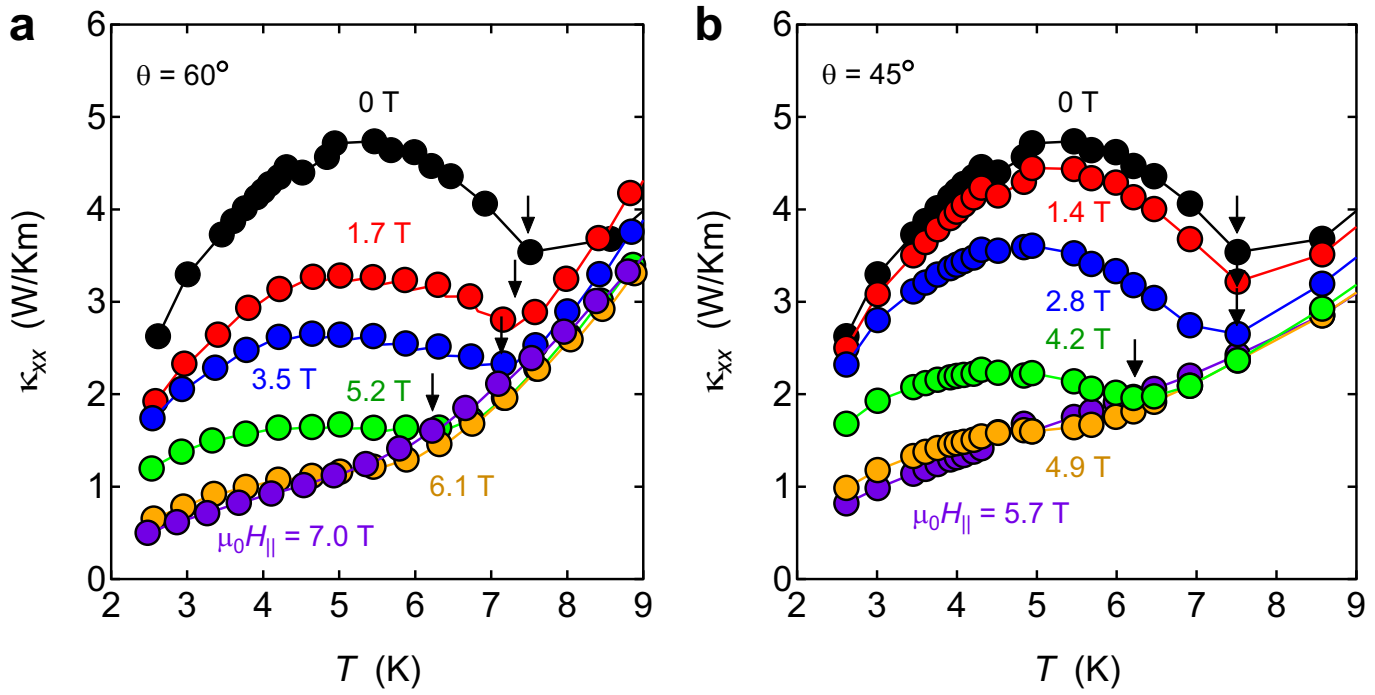

Extended Data Fig. 1 | Temperature dependence of the longitudinal thermal conductivity. a, **b**, κ_{xx} in a field tilted at $\theta = 60°$ (**a**) and 45° (**b**), plotted as a function of temperature (see inset of Fig. 2a). Arrows indicate the onset temperature of the AFM order T_N.

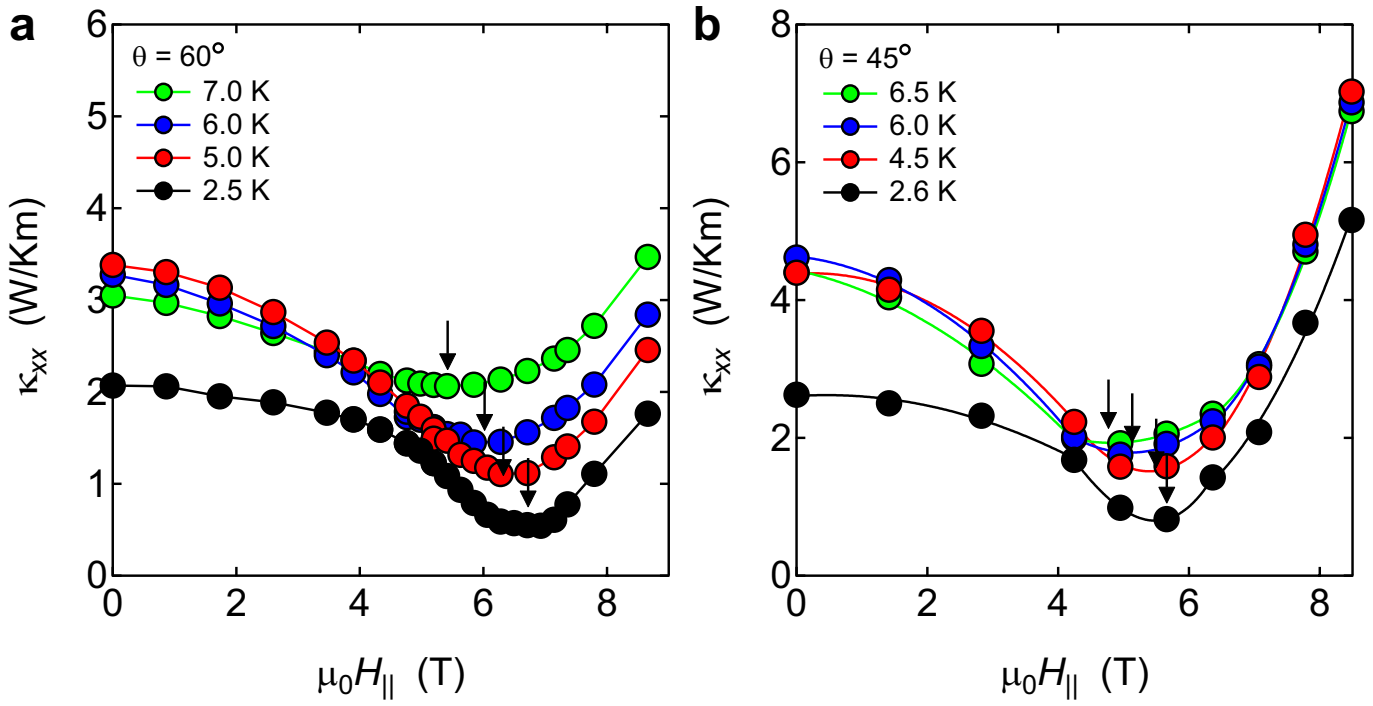

Extended Data Fig. 2 | Field dependence of the longitudinal thermal conductivity. a, **b**, κ_{xx} in field tilted at $\theta = 60°$ (**a**) and 45° (**b**), plotted as a function of the parallel field component $H_{\parallel}$ (see inset of Fig. 2a). Arrows indicate the minimum of κ_{xx}, which is attributed to the onset field of the AFM order.

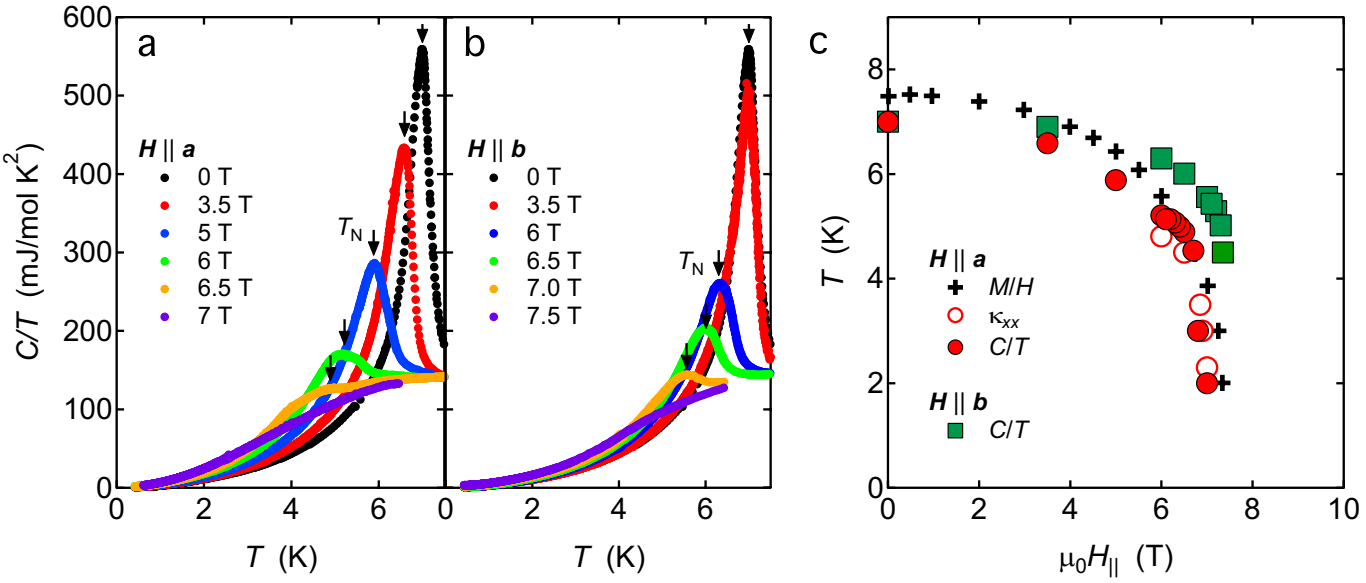

Extended Data Fig. 3 | Phase diagram of α-$RuCl_3$ for $H \parallel a$ and $H \parallel b$. **a**, **b**, Temperature dependence of the specific heat, C, divided by T for $H \parallel a$ (**a**) and $H \parallel b$ (**b**). Arrows indicate the Néel temperature T_N. **c**, Field dependence of T_N for $H \parallel a$ and $H \parallel b$, determined by the specific heat measurements. T_N, determined from the thermal conductivity and magnetic susceptibility[26], is also shown. The critical field for $H \parallel a$ is slightly lower than that for $H \parallel b$, but both phase diagrams are very similar.

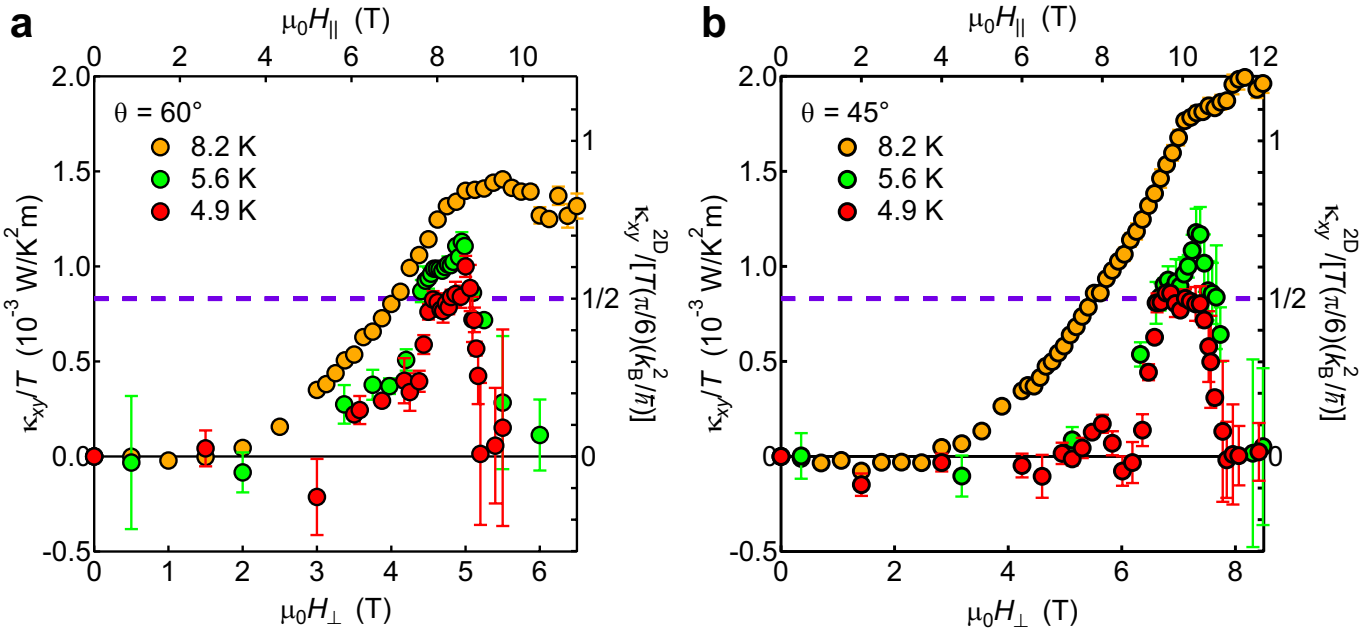

Extended Data Fig. 4 | Field dependence of thermal Hall conductivity. **a**, **b**, Thermal Hall conductivity, κ_{xy}/T, in a field tilted at $\theta = 60°$ (**a**) and 45° (**b**), plotted as a function of $H_{\perp}$ (see inset of Fig. 2a). The top axes show the parallel field component, $H_{\parallel}$. The right scales represent the 2D thermal Hall conductance, κ_{xy}^{2D}/T, in units of $(\pi/6)(k_B^2/\hbar)$. Violet dashed lines represent the half-integer thermal Hall conductance, $\kappa_{xy}^{2D}/[T(\pi/6)(k_B^2/\hbar)] = 1/2$. Error bars represent one standard deviation.

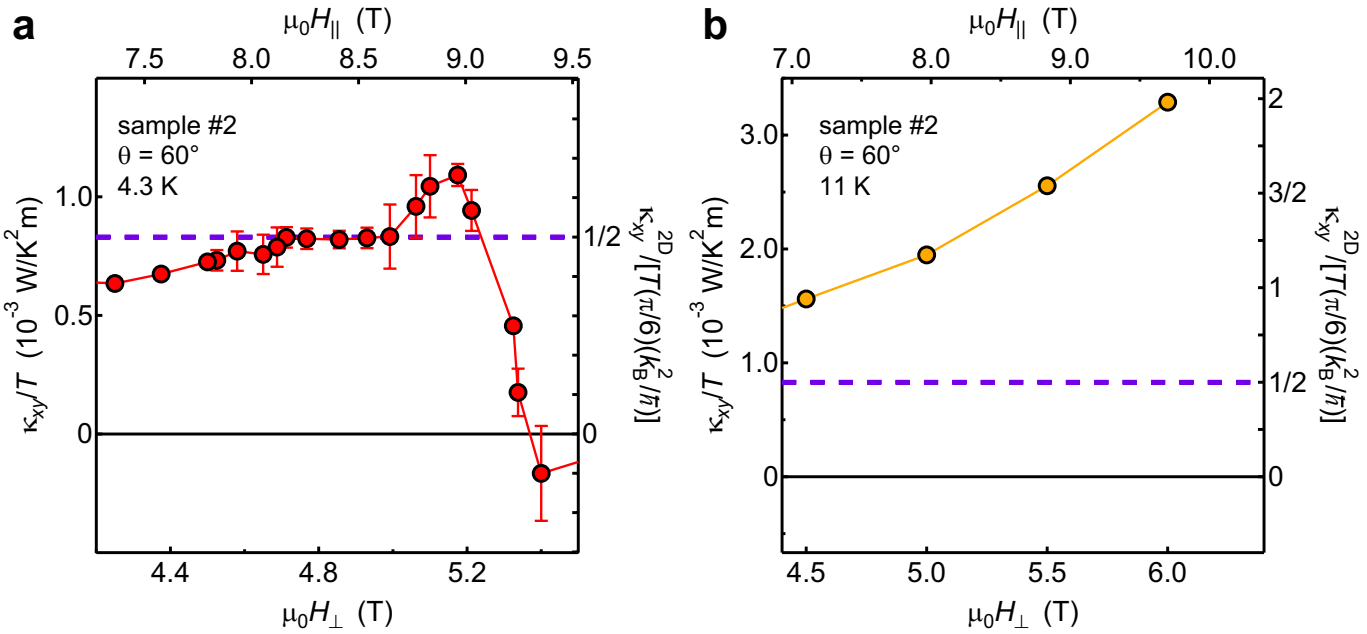

Extended Data Fig. 5 | Sample dependence of κ_{xy}. **a**, κ_{xy}/T measured in a different crystal (sample 2) for $\theta = 60°$ (see inset of Fig. 2a) at 4.3 K, plotted as a function of $H_\perp$. The right scales represent the 2D thermal Hall conductance, κ_{xy}^{2D}/T, in units of $(\pi/6)(k_B^2/\hbar)$. The half-integer thermal Hall conductance plateau is observed at $4.5\ \mathrm{T} < \mu_0 H_\perp < 5.0\ \mathrm{T}$. The field where the overshoot behaviour from the quantization value is observed is slightly higher than that of sample 1, but the field where κ_{xy}/T vanishes ($\mu_0 H_{||} \approx 9.3$ T) is close to that of sample 1. **b**, κ_{xy}/T of sample 2 in a field tilted at $\theta = 60°$, plotted as a function of $H_\perp$ at 11 K. Error bars represent one standard deviation.

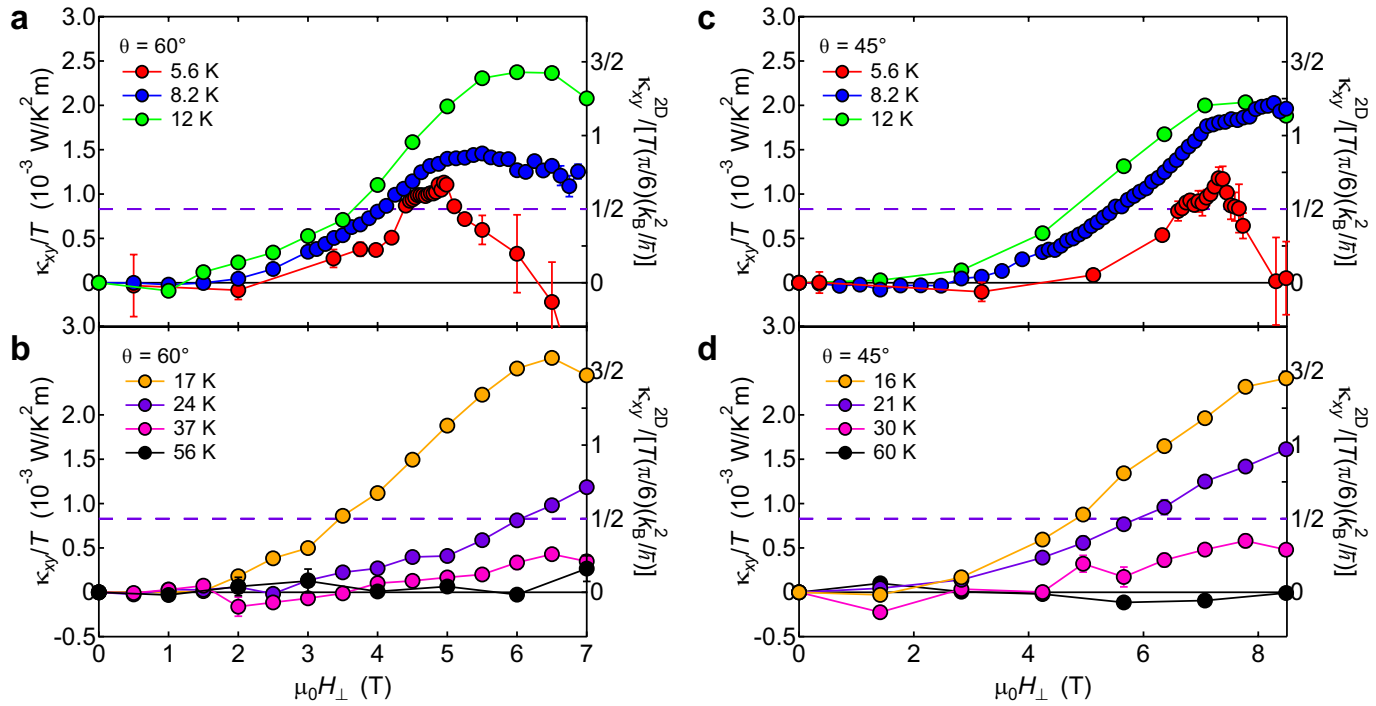

Extended Data Fig. 6 | Field dependence of thermal Hall conductivity in tilted fields at high temperatures. a–d, Thermal Hall conductivity, κ_{xy}/T, in a field tilted at $\theta = 60°$ (**a**, **b**) and 45° (**c**, **d**), plotted as a function of $H_\perp$, (see inset of Fig. 2a). The right scales represent the 2D thermal Hall conductance, κ_{xy}^{2D}/T, in units of $(\pi/6)(k_B^2/\hbar)$. Violet dashed lines represent the half-integer thermal Hall conductance, $\kappa_{xy}^{2D}/[T(\pi/6)(k_B^2/\hbar)] = 1/2$. Error bars represent one standard deviation.

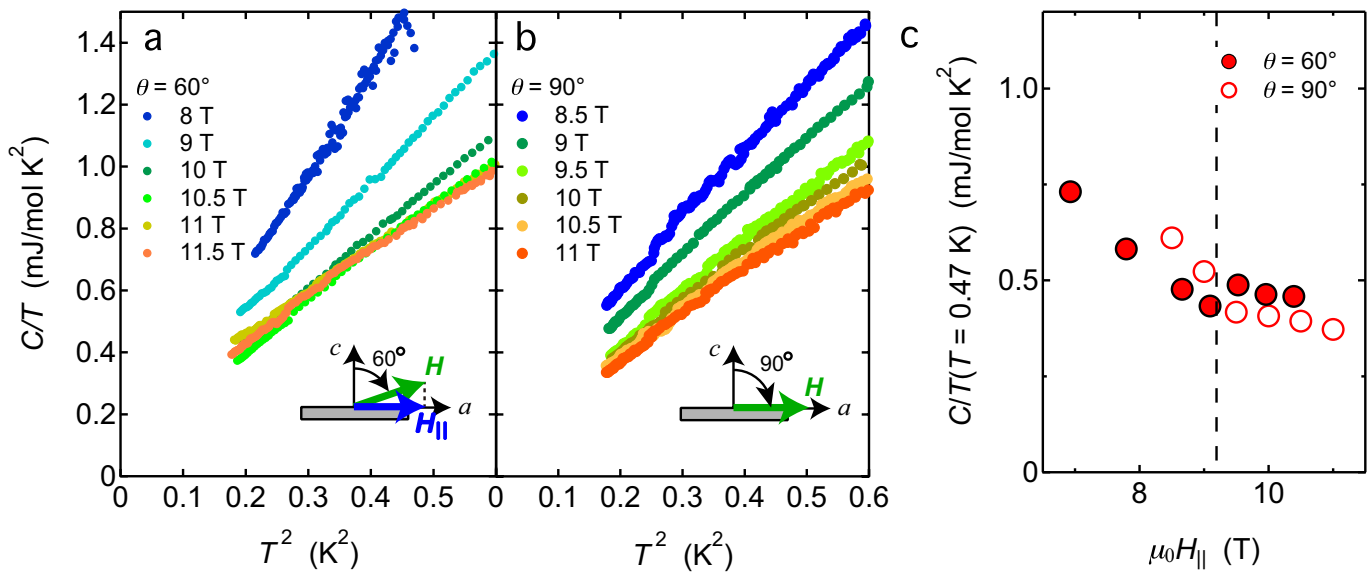

Extended Data Fig. 7 | Specific heat above $H_{\parallel}^{*}$. a, **b**, Temperature dependence of C/T for $\theta = 60°$ (**a**; $\boldsymbol{H}$ is tilted within the a–c plane) and 90° (**b**). **c**, C/T at 0.47 K plotted as a function of $H_{\parallel}$ for $\theta = 60°$ and 90°. $C(H)/T$ exhibits a dip-like anomaly for $\theta = 60°$ and a kink for $\theta = 90°$ at $\mu_0 H_{\parallel} \approx 9.2$ T (dashed line). This field almost coincides with the characteristic field at which κ_{xy}/T vanishes.